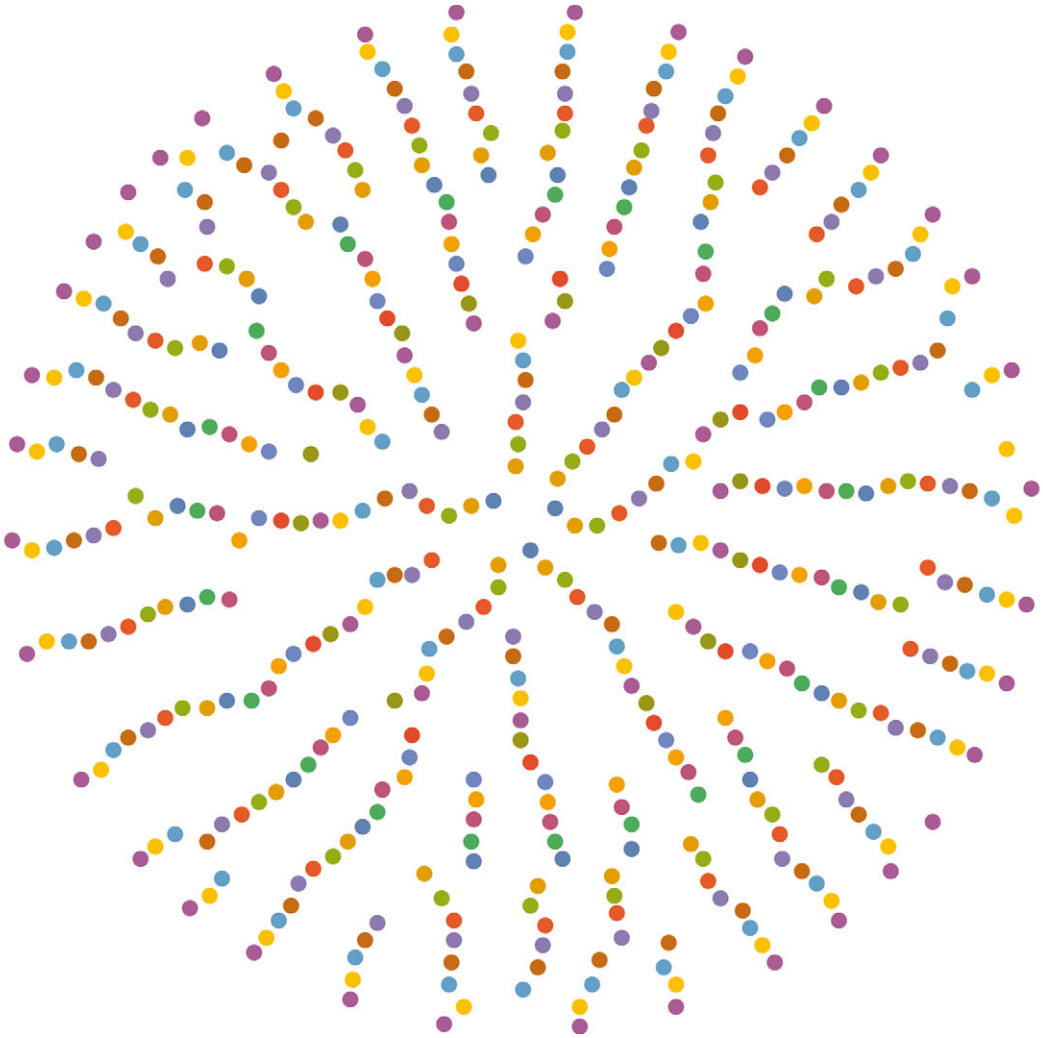

Highlighting research results from the University of Colorado, Boulder, USA

Capillary rupture of suspended polymer concentric rings

The correlated capillary instability amongst polymer concentric rings suspended on viscous medium was studied. Three modes of instability were identified: non-correlated, out-of-phase and in-phase. Most interestingly, the in-phase mode exhibited a fractal-like pattern (shown here). This pattern was attributed to frustrated capillary rupture in concentric ring geometry; a scaling law was developed to account for this behaviour.

As featured in:

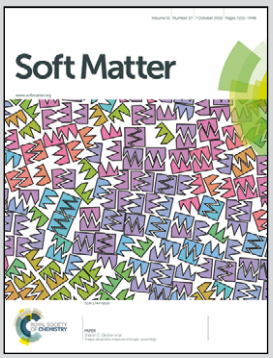

See Zheng Zhang, Yifu Ding *et al.*, *Soft Matter*, 2015, **11**, 7264.

ROYAL SOCIETY OF CHEMISTRY

www.softmatter.org

Registered charity number: 207890

Soft Matter

PAPER

View Article Online
View Journal | View Issue

Cite this: *Soft Matter*, 2015, **11**, 7264

Capillary rupture of suspended polymer concentric rings†

Zheng Zhang,*[a] G. C. Hilton,[b] Ronggui Yang[a] and Yifu Ding*[ac]

Received 22nd June 2015,
Accepted 12th August 2015

DOI: 10.1039/c5sm01537e

www.rsc.org/softmatter

We present the first experimental study on the simultaneous capillary instability amongst viscous concentric rings suspended atop an immiscible medium. The rings ruptured upon annealing, with three types of phase correlation between neighboring rings. In the case of weak substrate confinement, the rings ruptured independently when they were sparsely distanced, but *via* an out-of-phase mode when packed closer. If the substrate confinement was strong, the rings would rupture *via* an in-phase mode, resulting in radially aligned droplets. The concentric ring geometry caused a competition between the phase correlation of neighboring rings and the kinetically favorable wavelength, yielding an intriguing, recursive surface pattern. This frustrated pattern formation behavior was accounted for by a scaling analysis.

I. Introduction

Capillary instability is a commonly observed phenomenon: a slender liquid object ruptures into a series of droplets, driven by surface/interfacial tension (γ).[1] The droplets are spaced at a characteristic distance, corresponding to the fastest growing wavelength (mode). From Tomotika's linear stability analysis, this mode is a function of the interfacial tension and the cylinder-to-medium viscosity ratio.[2] When multiple cylinders are embedded in parallel within the same medium, the dominant mode for neighboring cylinders can become correlated:[3] the droplets positioned either in-phase or out-of-phase.[4]

Despite the rich literature on capillary instability of straight cylinders, studies on curved objects have been rather lacking until recent years. Pairam *et al.*[5] successfully created an unstable ring (toroid) by injecting liquid into a rotating bath of an immiscible liquid. They showed that the evolution of the as-formed ring was dictated by the competition between radial contraction and circumferential rupture.[5] Yao *et al.* analyzed the Stokes flow during the contraction.[6] Mehrabian *et al.* simulated both the contraction and the non-linear rupture of an embedded Newtonian ring.[7] The aforementioned literature suggests that the characteristic contraction time and rupture time predominantly scale with the medium viscosity and ring viscosity, respectively. Indeed, by replacing the medium with a highly viscoelastic material, the two timescales can be decoupled.[8] Furthermore, the stability of a substrate-supported liquid ring was studied both theoretically[9] and experimentally, *via* spin-coating,[10] solvent evaporation[11] and pulse-laser,[12,13] as well as ion-beam.[14]

Previous research has focused on a single ring; whether and how multiple closely arranged rings would rupture remained unclear. This could be because none of the literature methods were capable of creating multiple embedded rings, with well-defined dimensions and physical properties. Here, we report the first experimental study on capillary instability amongst suspended concentric rings.

II. Experimental

Polystyrene "PS35k" (average molecular weight $M_w \approx 35$ kg mol^{-1}, as determined with GPC; glass transition temperature $T_g = 95$ °C) was purchased from Sigma-Aldrich Co. LLC. Poly(methyl methacrylate) "PMMA15k" (average $M_w \approx 15$ kg mol^{-1}, as determined with GPC; $T_g = 88$ °C) was purchased from Scientific Polymer Products, Inc. Both polymers were used as received.

The concentric rings were created by a three-step fabrication process, which we developed previously.[15] A PMMA15k film was first spin-coated onto a silicon wafer substrate at 2000 rpm, from a 20 wt% solution in toluene. Prior to use, the wafer had been cleaned with oxygen plasma. The thickness of the film was determined from the step height measurement of a razor blade scratch, using atomic force microscopy (AFM, Dimension 3100, Bruker Corporation). We used Gwyddion for AFM image analysis.

An Eitre 3 nanoimprinter (Obducat, Inc.) was used to replicate micron-scale concentric ring patterns from a rigid silicon mold onto the PMMA films (Fig. 1a). The mold was fabricated *via* a standard Si micromachining protocol: exposing

[a] *Department of Mechanical Engineering, University of Colorado at Boulder, Boulder, Colorado 80309, USA. E-mail: zheng.zhang@colorado.edu, yifu.ding@colorado.edu*
[b] *National Institute of Standards and Technology, Boulder, Colorado 80305, USA*
[c] *Materials Science and Engineering Program, University of Colorado at Boulder, Boulder, Colorado 80309, USA*

† Electronic supplementary information (ESI) available. See DOI: 10.1039/c5sm01537e

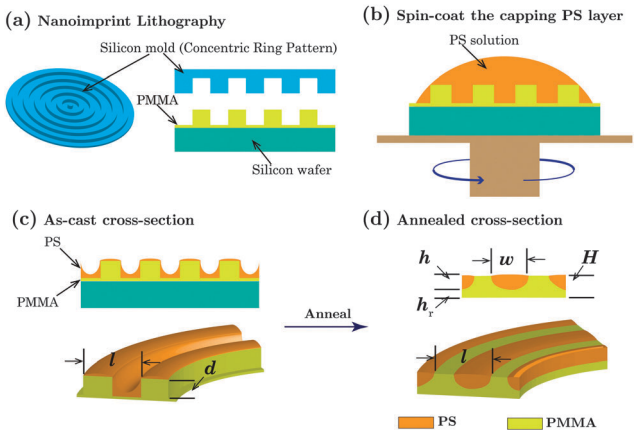

Fig. 1 Schematics of the fabrication procedures for suspended PS rings: (a) transfer concentric ring pattern from silicon mold to spin-cast PMMA film, *via* nanoimprint lithography; (b) spin-cast PS on top of the PMMA pattern; (c) cross-section of the as-cast bilayer film; (d) cross-section of the film after annealing.

the photoresist on wafer with a standard i-line wafer stepper and etching the Si using DRIE (deep reactive ion etcher) *via* "Bosch process". The pattern was replicated *via* the thermal-embossing mode of nanoimprint lithography (NIL), at 160 °C temperature and 4 MPa normal pressure for 20 minutes.

Subsequently, PS35k was spin-coated onto the PMMA pattern from an 8 wt% solvent in 1-chloropentane, a selective solvent for PS which would not deteriorate the bottom PMMA pattern during spin-coating (Fig. 1b). The bilayer film was then annealed *in vacuo* at 50 °C (below the T_g of PMMA) for 8 hours in order to remove residual solvent.

We then annealed the bilayer film at 170 °C on an STC200 microscopy hot-stage (Instec, Inc., temperature stability ±0.1 °C). At this temperature, both PS and PMMA turned into viscous fluids and the bilayer would form individual PS rings, suspended on the viscous PMMA medium. Both PS and PMMA were supported on Si substrate. The surface morphologies were observed *in situ* with an Olympus BX60 optical microscope, while the sample was being annealed at constant temperature. ImageJ was used to process the power spectrum density profiles, extract the average capillary wavelengths and calculate surface areas occupied by each phase.

III. Results and discussion

In this report, we show three representative samples (A, B and C), imprinted with molds with different pattern designs. Details of the polymers and the experimental processes are furnished in the Experimental section.

The cross-sectional geometry of the as-cast patterns is illustrated in Fig. 1c, where PS mostly segregated in the PMMA trenches. Being a non-minimum shape, the pattern would spontaneously evolve at a temperature above the T_gs of PS and PMMA.

At first, the corrugation was leveled by the vertical Laplace pressure, forming PS rings. The Laplace pressure exerted onto a linear grating pattern can be estimated by $P \approx 2\pi^2\gamma d/l^2$, where d and l are the height and periodicity of the corrugation, respectively.[16,17] Hereafter we refer to the PS rings as the "rings". The small dots between rings were produced by capillary rupture of PS originally atop the PMMA mesas, and did not exert much hydrodynamic influence due to size.[15] Fig. 1d schematically shows the cross-section of the rings, with w, h, h_r denoting the width and thickness of the ring, and the residual layer thickness, respectively (Table 1). Details of the leveling process can be found at ref. 15. In this report, we shall compare the morphological evolution of the concentric rings with Pairam *et al.*'s study on a single ring.[5] We stress that Pairam *et al.*'s observations were made on a freely suspended ring in an immiscible medium, whereas, in our system, there existed a solid Si substrate. By increasing h_r (*i.e.*, reducing substrate influence), we can direct our system to behave more similarly to Pairam *et al.*'s rings.

Table 1 Key geometric parameters of sample A, B and C, after the suspended PS rings had formed (Fig. 1d)

Sample	w [μm]	h [μm]	l [μm]	h_r [μm]	w/h	$2l/w$
A	3.1	1.0	20.2	1.1	3.1	13.0
B	4.6	1.4	12.1	1.7	2.7	5.3
C	8.5	1.6	25.0	0.5	5.3	5.9

The entire leveling process completed within the first minute of annealing, as the flow times of both polymers under P were very short: η_{PS} = 802 Pa s, and η_{PMMA} = 1450 Pa s, from our rheological measurements. Because of the low molecular weight of the polymers, we expect no influence of viscoelasticity. During this process, w of the rings decreased, in order to balance the surface tension of PS and the interfacial tension of PS/PMMA ($\gamma_{PS}/\gamma_{PS/PMMA} \approx 23$@160 °C).[15,18] The R of each ring and periodicity l remained nearly constant, indicating negligible contraction of the rings. The only exception was the innermost ring in Fig. 2a evolving into a single droplet in Fig. 2d. In this case, the shape evolution was not due to radial contraction: the ring ruptured first and then rounded up, which was also observed on fat rings by Pairam *et al.*[5]

Yao & Bowick analytically solved the contraction rate of a freely suspended ring (eqn (13) and (14) from ref. 6). We adapt their solution to our system and rewrite the rate as:

$$\frac{dR}{dt} = -\frac{\gamma_{PS/PMMA}}{6\eta_{PMMA}} \cdot \frac{p}{p^2 - \frac{1}{2}},$$

where $p = 2R/w$ is the aspect ratio of a ring. As a conservative estimate, we calculate the contraction rate of the fastest contracting ring (*i.e.*, the 2nd innermost ring) to be on the order of 10^{-3} μm s^{-1}, using the parameters at the onset of annealing: $\gamma_{PS/PMMA} \approx 1.38$ mN m^{-1}, $R \approx 28$ μm. At this rate, R would only decrease ~1 μm before the capillary rupture time of ~20 min (Fig. 2c), which was negligible in comparison with l. The rest of the rings had even larger p and, as a result, even smaller contraction rate. Here $w/2$ is considered equivalent to the tube radius (a) of a toroid. In following discussions, we will only

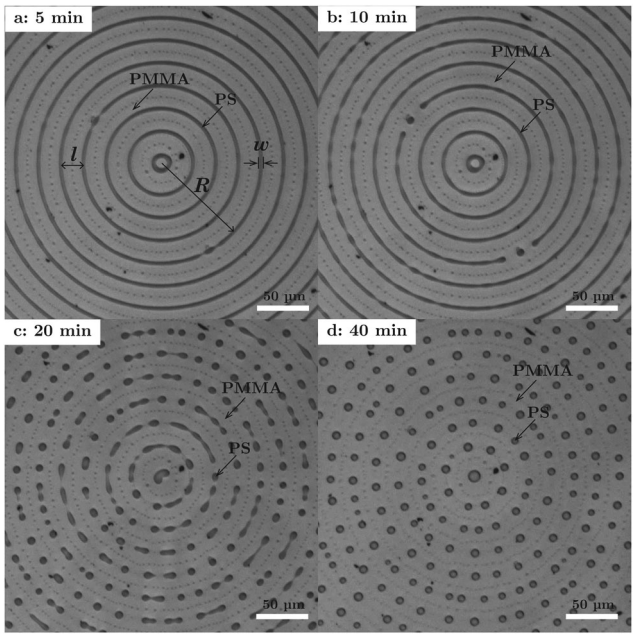

Fig. 2 Optical image of concentric PS rings (w = 3.1 μm, l = 20.2 μm, sample A) annealed at 160 °C for the labeled duration: (a) newly formed, (b) undulation, (c) rupture and (d) shape relaxation of individual droplets.

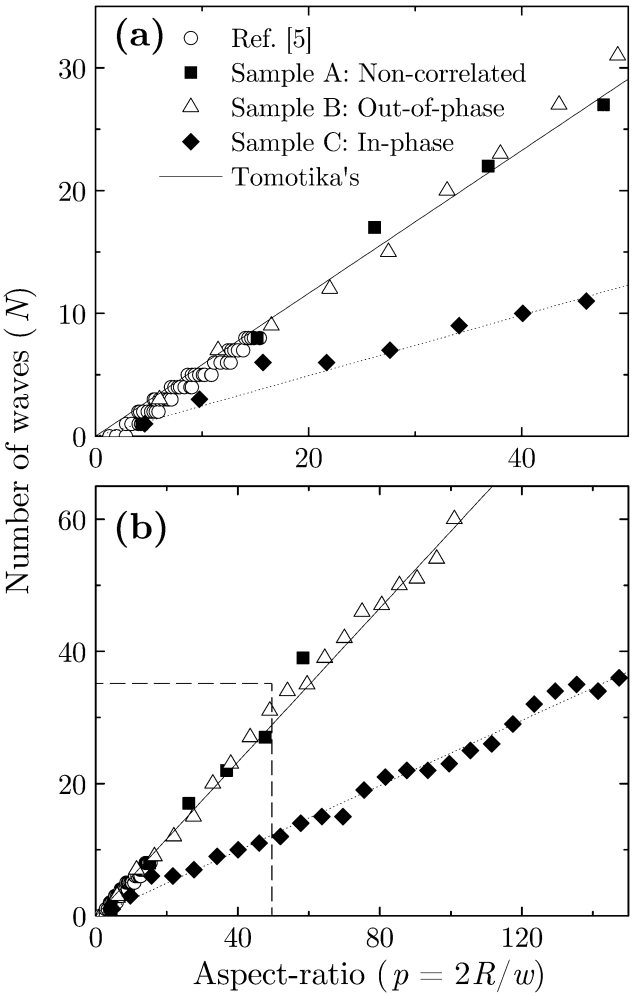

Fig. 3 The number of capillary wavelengths plotted as a function of aspect ratio. The solid line is based on Tomotika's theory. The dotted line is a linear fit to the "in-phase" data. The empty circles are adapted from ref. 5. (a) Magnifies the dashed line region of (b) for improved readability, whereas (b) shows the full range of data.

focus on the rupture behaviors of the rings, after the initial leveling process.

Fig. 2a shows sample A at 5 min of annealing, forming concentric rings with $w \approx 3.1$ μm, $h \approx 1.0$ μm, $h_r \approx 1.1$ μm and $l \approx 20.2$ μm. In order to capture the undulation stage of sample A, we used 160 °C as the annealing temperature, which was 10 °C lower than sample B and C. This small difference would not alter the pathway of morphological evolution. All the rings had identical w, which guaranteed $p \propto R$. The cross-section of each ring, represented by a ratio of $w/h \approx 3$, is consistent with that of straight filaments after the fast leveling process.[15,19,20] At this time, the rings in the PMMA trenches remained continuous (Fig. 2a), albeit periodic capillary fluctuations were already discernible (Fig. S1, ESI†). After 40 min, all rings had ruptured into discrete droplets (Fig. 2d). Note that the ruptured segments quickly equilibrated into droplets and were kinetically immobilized, because collision-based coalescence rate was extremely slow.[21] This was also observed in sample B (Fig. S2, ESI†).

We plot the number of wavelengths (N) from each ring as a function of p (solid squares in Fig. 3): a linear relationship can be found. Most interestingly, the slope of $N \sim p = 0.582$ is consistent with Tomotika's classical theory for the fastest growing mode of instability,[2] by applying Pairam *et al.*'s method of analogy to our viscosity ratio.[5] Since $p \propto R$, the linearity $N \propto p$ implies that the breakup wavelength $\lambda = 2\pi R/N \propto R/p$ was a constant for all the rings with sufficiently large p. We note that Fig. 3a only shows a limited range of p in order to faithfully reproduce the linearity of ref. 5's data points; a full range plot is provided as Fig. 3b. The linearity holds true for the entire sample surface. This is hardly surprising, since our rings possessed comparable or larger p than ref. 5 – intuitively, the larger p is, the more likely a toroid behaves like a straight cylinder.

Besides λ, we were also interested in the phase correlation between the rupture of neighboring rings. In Fig. 3a, our multiple rings exhibited consistency with a single ring as examined in ref. 5, suggesting that our multiple rings behaved as an ensemble of independent, isolated rings. To unambiguously identify the phase correlation, we statistically analyzed the coordinates of all the droplets formed. We define the phase shift (ϕ) locally for every droplet, as shown in Fig. 4a. For an arbitrary droplet X, we find its closest pair of droplets on the outer ring, Y and Z, and calculate central angles α and β. We define ϕ with an angular relationship: $\phi = 2\pi\alpha/\beta$.

For in-phase correlation, X aligns with either Y or Z along the radius (in-phase), so ϕ becomes 0 or 2π, respectively. For out-of-phase, $\alpha = \beta/2$ and, therefore, $\phi = \pi$. Fig. 4b is the distribution across the entire sample, suggesting a uniform distribution: the rings ruptured independently. This is not surprising, given that

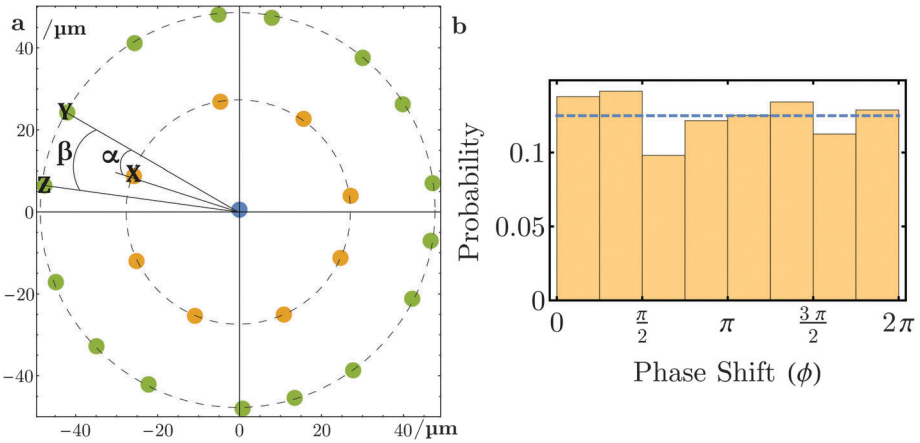

Fig. 4 (a) Schematic for defining phase shift (ϕ); (b) distribution of ϕ. The dashed line is the mean average of the bar heights.

neighboring rings are sparsely distanced ($2l/w \approx 13$). Knops *et al.* showed that for a viscosity ratio of 0.04 and 4, the flow induced by capillary rupture of a cylinder extended up to ~10 times its radius.[4]

In order to enhance the hydrodynamic interaction between neighboring rings, we fabricated sample B with reduced l, *via* the same procedure but with a different mold (12 μm periodicity, and a line-and-space ratio of 1). Upon annealing at 170 °C for 5 min, the surface leveling process was completed, resulting in a set of denser packed rings (Fig. 5a) than sample A (Fig. 2a). For sample B: $w \approx 4.6$ μm, $h \approx 1.4$ μm, $h_r \approx 1.7$ μm and $l \approx 12.1$ μm. The cross-section $w/h \approx 2.7$, again, reflected the balance between the γ_{PS} and $\gamma_{PS/PMMA}$. Most critically, the $2l/w$ ratio for sample B was ~5.3. Upon further annealing, the rings started to undulate and rupture (Fig. 5b). After 60 min, all rings had ruptured into discrete droplets (Fig. 5c), whose sizes and positions remained unchanged even after 540 min (Fig. S2, ESI†).

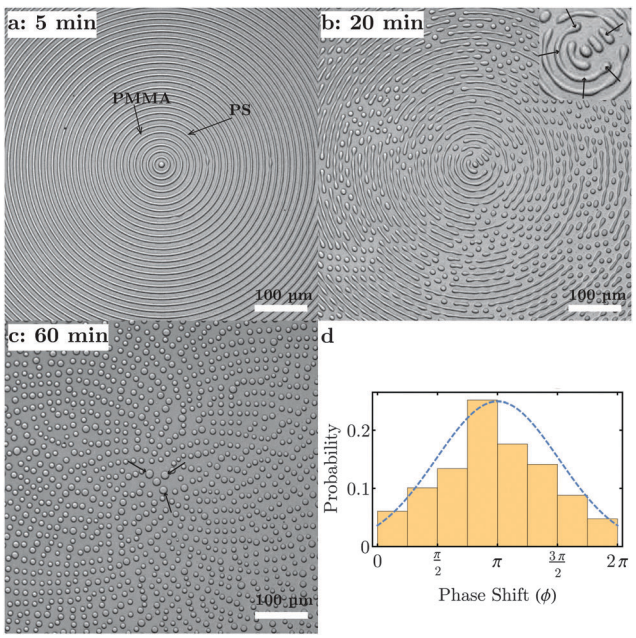

Fig. 5 Optical images of sample B annealed at 170 °C: (a) after leveling (w = 4.6 μm, l = 12.1 μm) and (b and c) rupture. (d) Distribution of ϕ. The dotted line is a fit to a truncated normal distribution within domain [0, 2π).

Similar as sample A, the $N \sim p$ relationship (empty triangles in Fig. 3a) matched Tomotika's theory.[2,5] The only exceptions are the two innermost rings, where in-plane relaxation dominated and reduced the number of droplets (arrows in Fig. 5b and c).

In stark contrast, Fig. 5d suggested a unimodal distribution, peaked near π. This unambiguously shows that the most probable phase correlation is out-of-phase. For this sample, the neighboring rings were sufficiently near ($2l/w \approx 5.3$) to interfere with each other. Based on recent numerical work, for a cylinder/medium viscosity ratio of ~1, out-of-phase correlation is expected for a $2l/w$ ratio of 3–10).[22] Sample A and B had a $2l/w$ ratio of 13.0 and 5.3, consistent with their non-correlated or out-of-phase mode, respectively.

From the previous studies on straight filaments,[3,4,15,19] the out-of-phase mode is the result of synchronized flow amongst neighbors: an alternation of necking and expanding occurred along the orthogonal direction. Therefore, N is constrained to be identical between neighbors. If this is also true for concentric rings, it would contradict the observed $N \propto p$ (Fig. 3a). We owe the observed linearity to the locality of the out-of-phase breakup, since there was no indication of long-range correlation/influence across sample B surface (Fig. 5b and c). The correlation became more evident starting from the 6th ring (Fig. S3, ESI†). This also resulted in a broadened distribution of ϕ.

Further decreasing the spacing between neighbors could transition the correlation into "in-phase", when the axial flow started to couple amongst neighbors.[4,22] This was also observed in sheared polymer blends.[23] From the recent numerical work,[22] we expect the threshold of $2l/w$ for out-of-phase to in-phase transition to be ~3, for our system (viscosity ratio of ~0.55). However, fabricating so densely-packed rings turned out rather challenging: simply increasing the cast volume of PS (higher concentration or low spin speed) would only result in a thick top layer, which levels into a planar bilayer during annealing, as opposed to forming concentric rings.[15]

We recently discovered that strongly confined straight filaments (*e.g.* small h_r) always break up in-phase, regardless of the viscosity ratio or the substrate wettability.[24] Herein, we fabricated substrate confined rings (sample C). The degree of confinement can be defined as H/h, where H is the overall film thickness (Fig. 1d). The smaller H/h is, the stronger substrate confinement is. The H/h for sample A (Fig. 2) and B (Fig. 5) were 2.1 and 2.2, respectively; both were larger than the bulk-to-confinement threshold of 2.0.[25] Therefore, both cases can be considered as weakly confined.

Fig. 6 shows sample C (see Fig. S4, ESI† for more snapshots). After the initial surface leveling within 5 min (and stable up to 180 min), $w \approx 8.5$ μm, $h \approx 1.6$ μm, $h_r \approx 0.5$ μm, $l \approx 25.0$ μm. For sample C, $H/h = 1.2$, meaning substrate exerted strong confinement on the rings. Its $w/h \approx 5.3$, indicating a flattened ribbon shape, that deviated significantly from the equilibrium shape ($w/h \approx 3$) of a weakly confined thread. The cross-sectional geometry as measured with AFM can be found in Fig. S7 (ESI†).

These confined rings were much more kinetically stable: they started to rupture between 400–600 min, which was more than one order of magnitude slower than sample A and B (Fig. 6a).

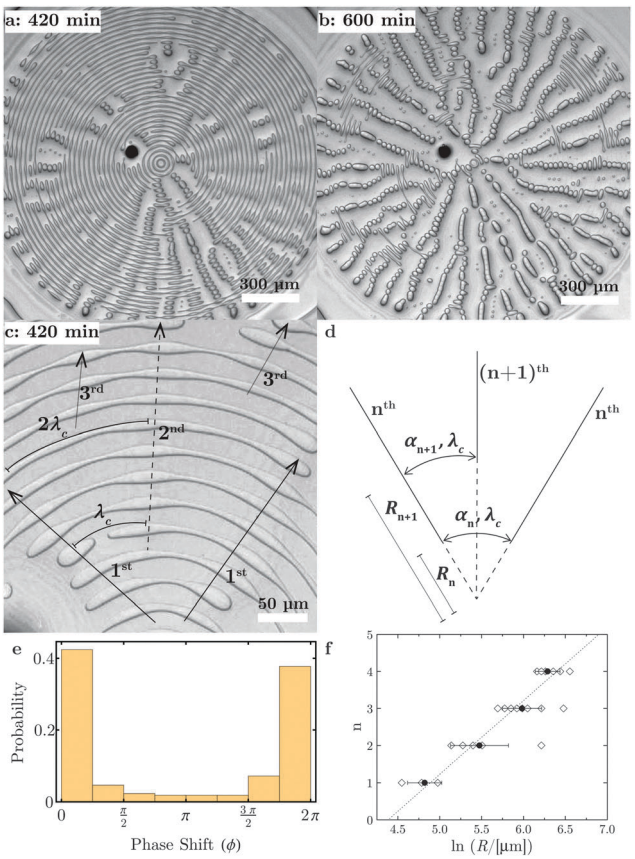

Fig. 6 (a and b) Optical images of sample C annealed at 170 °C for the labeled durations. Before undulation, $w = 8.5$ μm, $l = 25.0$ μm. (c) Close-up view of the undulation. (d) Schematic for the recursively "inserted" waves. (e) Distribution of ϕ. The analysis was performed on the undulation stage (420 min). (f) Scaling between the order of generation n and R. Empty diamonds represent every new wave. The dotted line is a linear fit.

The difference cannot be adequately explained by their difference in w. This is consistent with literature showing suppressed capillary instability under confinement.[23,26,27] Recent work by Alvine *et al.* also showed that the capillary fluctuations of polymer melt were dramatically hindered atop a topographic Si grating.[28]

Despite the slow kinetics, the rings eventually ruptured (Fig. 6b). However, different from straight filament arrays,[15,24] these droplets radially lined up. We plot the $N \sim p$ scaling (diamond symbols) in Fig. 3. The linearity again indicates constant λ for all rings. A linear fit (dotted line) shows that the slope (0.25) is less than half of Tomotika's theory. This directly translates to larger wavelength and droplet size by volume conservation.

As previously discussed, for concentric rings, $N \propto p$ (also observed in two other strongly confined patterns, Fig. S5, ESI†). Apparently, more waves had been "inserted" into the outer rings. Here we attempt to shed light upon this process. Fig. 6c shows the undulation. The primary correlated directions are marked "1st (generation)", extending radially from the center and perpendicular to the tangential of the rings. Moving away from the center, more waves were "inserted" in between the primary directions. Although the PS segments enveloped between "1st" directions all had the same central angle, their arc length (also λ) increased with R. The increased λ required a gradually less favorable undulation mode and built up the level of frustration. When this frustration grew sufficiently large, it could be released by inserting an additional wave in between (marked "2nd" in Fig. 6c). Similarly, the 3rd generation can be found at an even larger R. Therefore, the most energetically favorable (least amount of frustration) mode should correspond to the smallest λ. We denote this characteristic wavelength with λ_c. The upper bound of λ should be the most frustrated wavelength $2\lambda_c$ (on the verge of splitting up into two waves). It is always an abrupt change in λ from $2\lambda_c$ to λ_c, every time a new wave is inserted. Therefore, the average wavelength ranges within two bounds $\lambda_c < \lambda < 2\lambda_c$. We attribute the "waviness" of the in-phase data in Fig. 3b to this characteristic of λ.

λ_c can be directly measured by identifying the smallest wavelength, as labeled in Fig. 6c. We obtained that $\lambda_c = 77.8 \pm 11.0$ μm and the average $\lambda = 108.9 \pm 7.0$ μm, which was consistent with the lower and upper bound limit. Tomotika's theory provides a wavelength estimate of 45.9 μm. However, the lower bound λ_c was larger than the prediction, due to confinement-induced wavelength increase.[25,27]

We develop a scaling relationship to capture the recursive nature of the "insertion" behavior. As shown in Fig. 6d, in between the n^{th} generation envelope (radius R_n, central angle α_n, wavelength λ_c), a new wave is inserted in the middle but at a larger radius R_{n+1}. Therefore, $\forall n \in \mathbb{N}$:

$$\left.\begin{aligned} \alpha_n &= \frac{\alpha_1}{2^{n-1}} \\ R_n\alpha_n &= \lambda_c \end{aligned}\right\} \Rightarrow R_n = \frac{\lambda_c}{2\alpha_1}\cdot 2^n \propto 2^n,$$

or equivalently $\ln R_n \propto n$. We statistically verify the scaling against the experimentally observed order of generation n and $\ln R_n$ (Fig. 6f and Fig. S6, ESI†). The dotted line is a fit to the

mean value of $\ln R_n$ for each generation (n). The excellent linearity proves that, despite the randomness of surface capillary instability, our simple scaling analysis was capable of capturing the essential ''recursive'' behavior of the concentric rings. As a clarification, we have included every insertion of new wave in Fig. 6. However, since some insertions bore the same n and R, the number of data points in the plot appears less than the actual number of new waves.

IV. Conclusions

In summary, we developed a novel procedure that allowed us to examine capillary breakup of concentrically arranged PS rings, suspended atop a layer of PMMA. When the substrate confinement was weak, the rings broke up independently if they were far apart, but *via* an out-of-phase mode if they were sufficiently close. For both cases, the breakup wavelength agreed well with the prediction by Tomotika's linear stability theory for a fully embedded cylinder (approximating the ring half-width as the cylinder radius). Under significant confinement of the substrate, the rings tended to breakup *via* an ''in-phase'' mode along the radial direction. The unique concentric ring geometry induced strong geometric frustration, which yielded a self-similar morphology that could be accounted for by our scaling analysis. Geometric frustration associated with curvature is a fundamentally important topic. Our experiments can serve as a basis for correlated capillary instability among curved objects, which can be a powerful tool for creating unique surface patterns.

Acknowledgements

This work was supported by the National Science Foundation under Grant CMMI-1031785, CMMI-1233626 and CBET-1264276. ZZ acknowledges support from the Beverly Sears Graduate Student Grant at CU-Boulder.

References

1 J. Eggers and E. Villermaux, *Rep. Prog. Phys.*, 2008, **71**, 036601.
2 S. Tomotika, *Proc. R. Soc. London, Ser. A*, 1935, **150**, 322.
3 P. H. M. Elemans, J. M. van Wunnik and R. A. van Dam, *AIChE J.*, 1997, **43**, 1649.
4 Y. M. M. Knops, J. J. M. Slot, P. H. M. Elemans and M. J. H. Bulters, *AIChE J.*, 2001, **47**, 1740.
5 E. Pairam and A. Fernández-Nieves, *Phys. Rev. Lett.*, 2009, **102**, 234501.
6 Z. Yao and M. J. Bowick, *Eur. Phys. J. E: Soft Matter Biol. Phys.*, 2011, **34**, 32.
7 H. Mehrabian and J. J. Feng, *J. Fluid Mech.*, 2013, **717**, 281.
8 E. Pairam, H. Le and A. Fernández-Nieves, *Phys. Rev. E: Stat., Nonlinear, Soft Matter Phys.*, 2014, **90**, 021002.
9 A. G. González, J. A. Diez and L. Kondic, *J. Fluid Mech.*, 2013, **718**, 246.
10 J. D. McGraw, J. Li, D. L. Tran, A.-C. Shi and K. Dalnoki-Veress, *Soft Matter*, 2010, **6**, 1258.
11 M. Byun, S. W. Hong, F. Qiu, Q. Zou and Z. Lin, *Macromolecules*, 2008, **41**, 9312.
12 Y. Wu, J. D. Fowlkes, P. D. Rack, J. A. Diez and L. Kondic, *Langmuir*, 2010, **26**, 11972.
13 T. D. Nguyen, M. Fuentes-Cabrera, J. D. Fowlkes, J. A. Diez, A. G. González, L. Kondic and P. D. Rack, *Langmuir*, 2012, **28**, 13960.
14 J. Lian, L. Wang, X. Sun, Q. Yu and R. C. Ewing, *Nano Lett.*, 2006, **6**, 1047.
15 Z. Zhang, D. U. Ahn and Y. Ding, *Macromolecules*, 2012, **45**, 1972.
16 Y. Ding, H. W. Ro, K. J. Alvine, B. C. Okerberg, J. Zhou, J. F. Douglas, A. Karim and C. L. Soles, *Adv. Funct. Mater.*, 2008, **18**, 1854.
17 Y. Ding, H. J. Qi, K. J. Alvine, H. W. Ro, D. U. Ahn, S. Lin-Gibson, J. F. Douglas and C. L. Soles, *Macromolecules*, 2010, **43**, 8191.
18 J. E. Mark, *Physical Properties of Polymers Handbook*, Springer, New York, 2nd edn, 2007.
19 D. U. Ahn, Z. Wang, R. Yang and Y. Ding, *Soft Matter*, 2010, **6**, 4900.
20 D. U. Ahn and Y. Ding, *Soft Matter*, 2011, **7**, 3794.
21 L. Sung, A. Karim, J. F. Douglas and C. C. Han, *Phys. Rev. Lett.*, 1996, **76**, 4368.
22 P. J. A. Janssen, H. E. H. Meijer and P. D. Anderson, *Phys. Fluids*, 2012, **24**, 012102.
23 N. S. Martys and J. F. Douglas, *Phys. Rev. E: Stat., Nonlinear, Soft Matter Phys.*, 2001, **63**, 031205.
24 Z. Zhang, L. Wang and Y. Ding, *Langmuir*, 2013, **29**, 3073.
25 J. G. Hagedorn, N. S. Martys and J. F. Douglas, *Phys. Rev. E: Stat., Nonlinear, Soft Matter Phys.*, 2004, **69**, 056312.
26 K. B. Migler, *Phys. Rev. Lett.*, 2001, **86**, 1023.
27 Y. Son, N. S. Martys, J. G. Hagedorn and K. B. Migler, *Macromolecules*, 2003, **36**, 5825.
28 K. J. Alvine, Y. Dai, H. W. Ro, S. Narayanan, A. R. Sandy, C. L. Soles and O. G. Shpyrko, *Phys. Rev. Lett.*, 2012, **109**, 207801.